Available online at www.sciencedirect.com

ScienceDirect

Acta Materialia 64 (2014) 72–77

Acta MATERIALIA

www.elsevier.com/locate/actamat

Capturing the complex physics behind universal grain size distributions in thin metallic films

R. Backofen [a], K. Barmak [b], K.E. Elder [c], A. Voigt [a,*]

[a] Institut für Wissenschaftliches Rechnen, Technische Universität Dresden, 01062 Dresden, Germany
[b] Department of Applied Physics and Applied Mathematics, Columbia University, New York, NY 10027, USA
[c] Department of Physics, Oakland University, Rochester, MI 48309-4487, USA

Received 29 August 2013; received in revised form 11 November 2013; accepted 11 November 2013
Available online 18 December 2013

Abstract

Grain growth experiments on thin metallic films have shown the geometric and topological characteristics of the grain structure to be universal and independent of many experimental conditions. The universal size distribution, however, is found to differ both qualitatively and quantitatively from classical curvature driven models of Mullins type, which reduce grain growth to an evolution of a grain boundary network, with the experiments exhibiting an excess of small grains (termed an "ear") and an excess of very large grains (termed a "tail") compared with the models. While a plethora of extensions of the original Mullins model have been proposed to explain these characteristics, none have been successful. In this work, large-scale simulations of a model that resolves the atomic scale on diffusive time scales, the phase field crystal model, are used to examine the complex phenomena of grain growth. The results are in remarkable agreement with the prior experimental results, recovering the characteristic "ear" and "tail" features of the experimental grain size distribution. The simulations also indicate that, while the geometric and topological characteristics are universal, the dynamic growth exponent is not.

Keywords: Grain growth; Size distribution; Phase field crystal; Scaling law

1. Introduction

Most metals, ceramics and minerals are polycrystalline materials containing grains of different crystal orientation. The size, shapes and arrangements of these grains strongly affect macroscale material properties, such as fracture, yield stress, coercivity and conductivity. In magnetic systems, for example, the coercivity (or magnetic "hardness") can change by four or five orders of magnitude with a change in grain size [1]. Thus, understanding and controlling polycrystalline structures is of great importance in the production of many engineering materials, and has motivated numerous experimental and theoretical studies of grain growth.

Grain growth in thin metallic films is one example where extensive research has been conducted. One very interesting experimental finding in such systems is that the grain size distributions and topological characteristics appear to be independent of many experimental conditions [2]. More specifically, it has been found that, for a large collection of Al and Cu thin films, a universal grain size distribution emerges that is independent of the substrate, annealing temperature, purity, thickness and annealing time. Unfortunately the universal distribution is qualitatively and quantitatively different from the results of extensive computational studies on grain growth (e.g. [3]), which are based on the original Mullins model [4]. In this model, the problem is reduced to the evolution of a two-dimensional grain boundary network by relating the normal velocity v_n to the curvature κ of the grain boundary, $v_n = \mu\gamma\kappa$, with mobility μ and surface tension γ, and

* Corresponding author.
E-mail address: axel.voigt@tu-dresden.de (A. Voigt).

1359-6454/$36.00
http://dx.doi.org/10.1016/j.actamat.2013.11.034

specifying the Herring condition [5] at triple junctions. Various attempts have been made to extend the original Mullins model and to include more realistic effects, such as interactions of the film with the substrate, anisotropy in the grain boundary energy and mobility, grain boundary grooving, and solute and triple junction drag (see Ref. [2] and the references therein). While these extensions have in some cases been shown to significantly alter the grain statistics, no single cause has been able to explain all of the experimental measured quantities, as discussed in Ref. [2]. This discrepancy raises the question of whether the underlying picture of an evolving smooth grain boundary network of the Mullins curvature-driven models is perhaps oversimplified.

In addition to the grain size distribution, the rate of growth of the average grain size has also been examined in detail. The original Mullins model and its extensions all seem to predict that the average grain size, represented by its radius $r(t)$, has a power law behavior of the form $\sim t^{1/2}$, which follows immediately from the linear relationship between grain boundary velocity and curvature. Experimentally, a much slower coarsening or even stagnation of grain growth in thin films is observed. This may be because the original Mullins model and its extensions ignore the crystalline structure of the grains, the dissipation due to lattice deformations and the Peierls barriers for dislocation motion. It is difficult to reconcile Mullins-type models with the atomistic features of grain boundaries, which (for low angles) can be seen as an alignment of dislocations, where the driving force for grain growth is the stress associated with dislocation motion. The differences of the description are shown schematically in Fig. 1.

2. Atomic considerations

Atomistic descriptions can incorporate the important physical features missing in the Mullins-type models and have led to some important observations. It has been shown that the complex dislocation structure along curved grain boundaries gives rise to a misorientation-dependent mobility [6]. Further studies indicate that grain boundaries undergo thermal roughening associated with an abrupt mobility change, leading to smooth (fast) and rough (slow) boundaries [7], which can eventually lead to stagnation of the growth process. The defect structure at triple junctions can lead to a sufficiently small mobility limiting the rate of grain boundary migration [8,9]. Also, tangential motion of the lattices is possible. For low-angle grain boundaries, normal and tangential motion are strongly coupled as a result of the geometric constraint that the lattices of two crystals change continuously across the interface while the grain boundary moves [10]. As a consequence of this coupling, grains rotate as they shrink, which leads to an increase in the grain boundary energy per unit length, although the overall energy decreases since the size of the boundary decreases [11–13]. Each of these phenomena can be simulated using molecular dynamics (MD) (see Ref. [14] for a review). However, to study the effect of these phenomena on scaling laws, grain size distributions or stagnation of growth requires a method which operates on diffusive time scales. For this reason, we choose to study the PFC model, which incorporates atomistic details on diffusive time scales.

3. PFC model

The PFC method [15] was introduced to model elasticity, dislocations and grain boundaries in polycrystalline systems in a simple and natural fashion. The model has been shown to successfully model grain boundary energies as a function of misorientation [16] and non-classical grain rotation during grain shrinkage and drag of triple junctions [17]. In addition, lower coarsening exponents have been observed for hexagonal lattices [18–20], and even stagnation of grain growth could be seen [21]. The aim of this paper is to use the PFC model on large scales to obtain statistical data for grain size distributions and to compare them with prior experimental data for thin metallic films. Since the experimental results in Ref. [2] seem to be universal, we do not fit the PFC parameters to a specific material

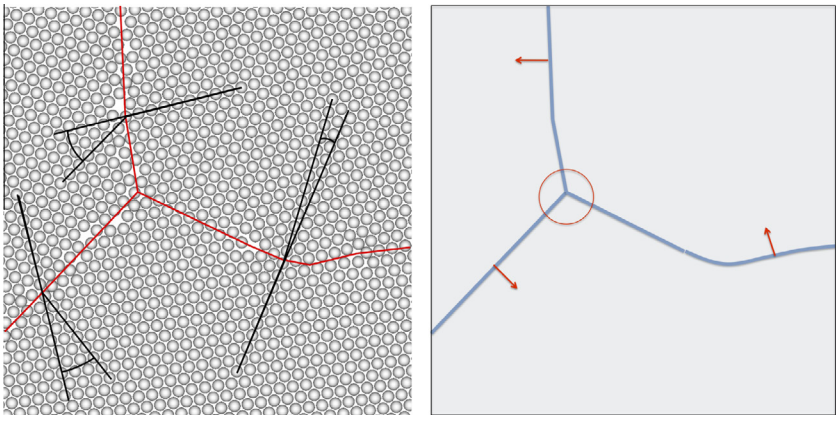

Fig. 1. Schematic comparison between an atomistic description of a polycrystalline material and a coarse-grained picture of a smooth grain boundary network. Shown is a low-angle grain boundary with aligned dislocations and two high-angle grain boundaries in an otherwise hexagonal lattice.

but consider an artificial setting within the simplest PFC model introduced in Ref. [15]. In dimensionless form, the equation reads

$$\frac{\partial \psi}{\partial t} = \Gamma \nabla^2 \frac{\delta \mathcal{F}}{\delta \psi} \tag{1}$$

where the order parameter ψ is related to the time-averaged atomic density, t is time, Γ is the mobility and $\mathcal{F}$ is the free energy, given by

$$\mathcal{F} = \int \psi\left(-\epsilon + \left(\nabla^2 + 1\right)^2\right)\frac{\psi}{2} + \frac{\psi^4}{4}\, dr \tag{2}$$

Here, ϵ is a parameter related to temperature. The free energy functional is constructed so that it is minimized in the liquid state by $\psi =$ constant and in the solid crystalline state by a periodic function that has triangular symmetry in two dimensions and a dimensionless lattice constant $4\pi/\sqrt{3}$. The precise phase diagram can be found in Ref. [15] and a small portion is shown in Fig. 3. In the crystalline state, $\mathcal{F}$ is minimized by a periodic function of arbitrary orientation, making the model ideal for the study of polycrystalline materials. Elasticity is naturally incorporated in this model as any deviation from the equilibrium triangular structure increases the energy. The specific elastic constants are controlled by the average density of $\psi, \bar{\psi}$ and ϵ, and can be written as $C_{12} = C_{44} = C_{11}/3$, where $C_{12} = [(3\bar{\psi} + \sqrt{15\epsilon - 36\bar{\psi}^2}/75$. This model and the parameters that enter it can be related to more fundamental approaches, such as classical dynamic density functional theory [22–24,16].

4. Results

Fig. 2 shows a snapshot of a typical simulation. The corresponding animations of the growth process are shown in the Supplementary material, as movies 1–3. The movies allow us to identify all of the mentioned effects resulting from the atomistic description, in particular fast and slow moving grain boundaries, pinned triple junctions, rotating grains, elastic deformations within single grains and the movement of isolated dislocations.

All simulations are performed in a periodic domain of square size $L = 8192$m starting from a randomly perturbed constant value of the particle density ψ. After an initiation phase in which the white noise is damped rapidly, grains nucleate, grow and impinge on one another. Thereafter, the number of maxima in the particle density ψ remains mainly constant and coarsening starts. Statistical results are collected after grains have reached a minimal size of 100 atoms.

4.1. Scaling results

Fig. 3 shows the obtained scaling results for the average domain area as a power law in time, i.e. t^q, where q is $1/2$ in the Mullins-type curvature-driven models. In our simulations it is not clear that this relationship is valid, as the value of q can be see to change in time and is dependent on the parameters of the simulation and initial conditions. For case "A", we either obtain an initial value of $q = 1/3$, which turns into $q = 1/5$, or a constant value of $q = 1/5$, depending on the initial grain size. The constant scaling exponent is observed for larger initial grains. For case "B", corresponding to a softer material, the growth exponent increases to a value of $q = 2/5$, whereas for case "C", a harder material, it decreases to $q = 1/20$. For all three cases, the growth exponent is significantly lower than the expected value $q = 1/2$ for the Mullins-type models. Similar low coarsening exponents have been found for hexagonal lattices in Refs. [18,19] and in experiments for thin films of CoPt and FePt [25]. Extensive computational studies in Refs. [19,20] further show a strong dependency of the scaling exponent on additional noise, which enhances the coarsening process. It has also been noted [20] that the addition of higher-order time derivatives can change the growth exponent, which may be appropriate for three-dimensional samples. In two-dimensional thin films (i.e. films with columnar grain structures), however, it is expected that the substrate/film coupling provides an effective friction for rotation or translation that eliminates the need for such corrections. In either case, it is likely that the growth exponents are transient because, for very large

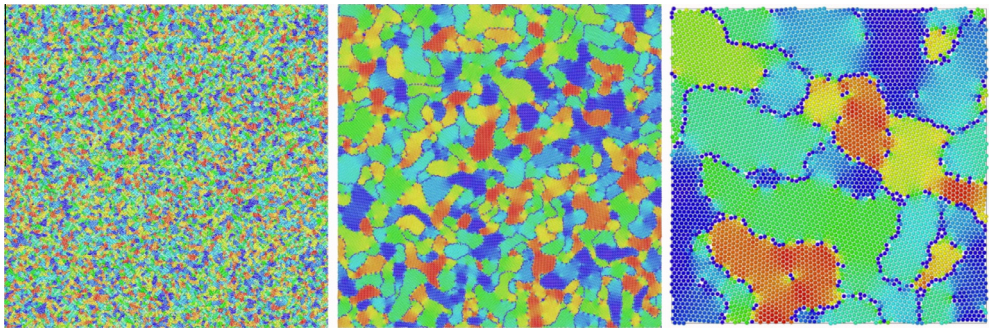

Fig. 2. Grain structure obtained from post-processing a phase field crystal (PFC) simulation at an intermediate time. The color coding indicates the averaged local lattice orientation for each of the maxima in the density field. An enlargement by a factor of four is used for each figure. Animations of the grain growth process for the three enlargements are provided in the supplementary materials, as movies 1–3, corresponding to case "A1" in Fig. 3. (For interpretation of the references to color in this figure legend, the reader is referred to the web version of this article.)

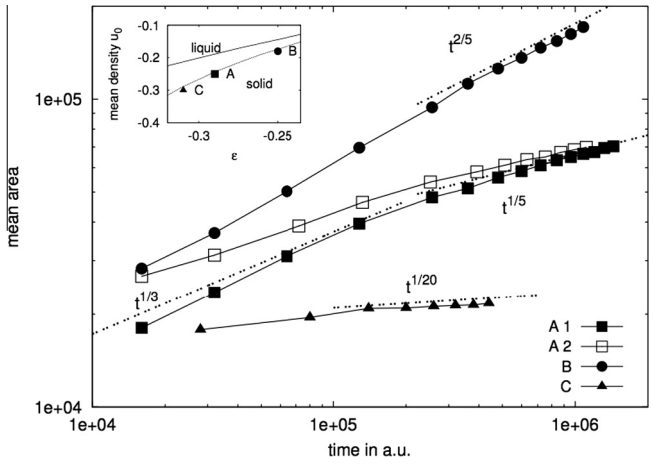

Fig. 3. Mean area as a function of time together with the fitted scaling exponents for various points in the phase diagram depicted in the inset. "A1" and "A2" have different initial grain sizes (A1 < A2). The parameters are "A": $(\psi_0, \epsilon) = (-0.29, -0.25)$; "B": $(\psi_0, \epsilon) = (-0.25, -0.18)$; "C": $(\psi_0, \epsilon) = (-0.31, -0.30)$.

grain sizes, the Peierls–Nabarro barriers are likely to inhibit further coarsening. This effect already occur at early times for quenches to lower temperatures, as confirmed for points in the phase diagram in the solid region at $(\psi_0, \epsilon) = (-0.31, -0.25)$, and $(\psi_0, \epsilon) = (-0.29, -0.18)$, which show a frozen configuration.

4.2. Grain-size distribution

While it is not entirely clear if there is a single, well-established dynamical exponent, the grain size distribution functions appear to be much more robust. Fig. 4 shows the averaged grain size distribution of the PFC simulations for the considered points in the phase diagram, together with

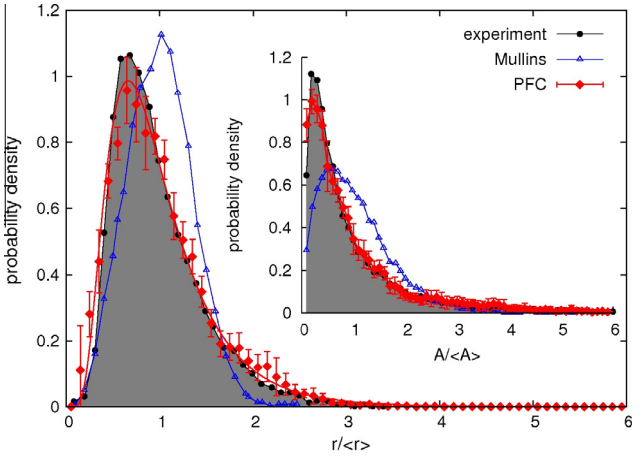

Fig. 4. Grain size distribution with reference to radius (area in inlet). Shown is the mean distribution, obtained as the average of the last time steps for cases "A1", "A2" and "B" in Fig. 3. Case "C" was not included as it may still contain remnants of the initial condition. The curve is fitted to a log-normal distribution with parameters $(\mu, \sigma) = (-0.13, 0.53)$. The experimental data and the results of the Mullins model are taken from Ref. [2].

the experimental results and the results of the Mullins-type model taken from Ref. [2].

A considerable discrepancy between the experimental results and the Mullins-type models has already been discussed in Refs. [26,2]. They differ in two important respects. First, the experimental grain structures have a larger number of small grains, as evidenced by the peak of the experimental reduced area probability density residing to the left of that for the simulations based on the Mullins-type models, a feature that has been termed the "ear". Second, the experimental grain structures have "tails" that extend to significantly larger sizes than those seen in simulations based on the Mullins-type models. While only very few grains seen in simulations exceed four times (and very rarely five times) the mean area, the experimental grain structures exhibit maximum grain areas that are between 8 and 42 times the mean, with a sizable fraction of grains whose areas exceed four times the mean grain area ($\sim 3\%$ by number, representing $\sim 18\%$ of the total area). Various closed-form distributions have been proposed to fit the results of the Mullins-type models, e.g. the Louat, Hillert, Rios and Weibull distribution (see Ref. [3] and the references therein). They all not only differ in the "ear" and "tail" regions, but also peak at $r/\langle r \rangle > 1$, again in disagreement with the experimental results. The PFC simulations not only recover the qualitative behaviour of the experimental results, they almost perfectly fit the distribution, and can be very well described by a log-normal distribution. The grain size distribution appears to be self-similar. This is analyzed in detail for case "A1" in Fig. 5. All of the results were obtained without additional noise. However, simulations that included noise (not shown) produced grain distributions consistent with the zero noise case. Further analysis indicates that, also in agreement with the experimental data, small grains are primarily three- and four-sided, whereas large grains generally have more than six sides.

5. Conclusions

The importance and prevalence of the formation and properties of polycrystalline materials has led to an enormous amount of theoretical and experimental research. Unfortunately theoretical progress has been hindered by the lack of computational methods that can capture the essential physics on the times and lengths that are appropriate for such phenomena. While MD simulations are currently unable to reach time scales required to observe self-similar growth regimes, coarse-grained descriptions based on the Mullins model seem to lack the essential atomistic features allowing for bulk dissipation during grain growth. In this work, large-scale numerical simulations of the PFC model were used to examine the phenomenon of grain growth in two-dimensional systems. The results of these simulations are in remarkable agreement with universal aspects of the geometric and topological characteristics of the grain structures in thin

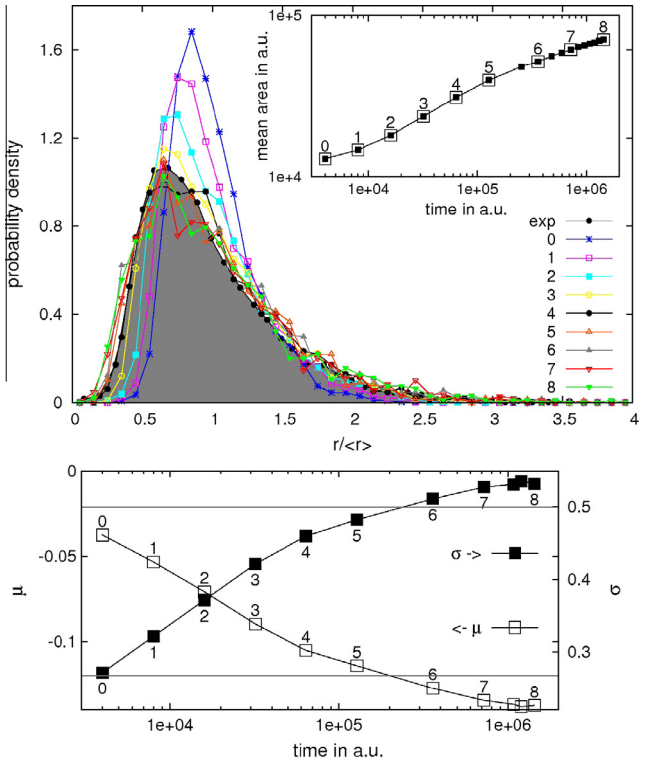

Fig. 5. (top) Grain size distribution with reference to radius at the labeled times in the inlet, corresponding to case "A1" in Fig. 3, in comparison with the experimental results from Ref. [2]. We choose the case with a "fast" coarsening rate to rule out any dependency on the initial conditions. The evolution for cases "A2", "B" and "C" are similar. The initially narrow distribution broadens rapidly and its peak shifts towards smaller grains. For large times the grain size distribution appears to be self-similar, which is further illustrated in the bottom image, which shows the time evolution of the parameters σ and μ of a log-normal distribution fitted to the considered snapshots, again in comparison with the experimental results from Ref. [2] (shown as the horizontal solid lines).

metallic films. Among other features, they capture both the "ear" and "tail" characteristics of grain distributions, which have proven difficult to obtain with previous models and methods. Thus the PFC model provides a key resource for future research in which realistic grain structures are required. Although not examined in this work, the model also incorporates mechanical properties of the system and thus can be used to study, for example, the relationship between growth conditions and the structural stability of polycrystalline materials.

6. Methods

6.1. Simulations

The computational approach is based on a modified version of the convexity splitting proposed in Ref. [27], which allows for a linearly implicit discretization and a highly efficient Fourier ansatz, which is solved in parallel on the high-performance computer JUROPA at FZ Jülich (www.fz-juelich.de/jsc/juropa). We identify the maxima in ψ, compute nearest neighbor relations according to the proposed approach in Ref. [28] and use OVITO (www.ovito.org) to plot the atomic arrangement with a color coding according to the number of neighbors to identify dislocations and the orientation for regular lattice points. Grain boundaries are then identified according to the presence of dislocations and a jump in orientation. In order to rule out numerical effects, the simulations have also been considered on different domains $L = 1024, L = 2048$ and $L = 4096$ to test for finite size effects, which are already absent for $L = 4096$. $L = 8182$ is used to obtain better statistics. We further varied the criteria to identify grain boundaries. Our results are not sensitive to these variations.

6.2. Experiments

The considered experimental data are for Al and Cu films, which were sputter deposited onto oxidized Si wafers or single crystal rock salt. The Al films were deposited at nominally room temperature, while the Cu films were deposited at −40 °C. The Cu films were encapsulated in sputter-deposited SiO_2 or $Ta_{38}Si_{14}N_{48}/SiO_2$. Following deposition, the films were annealed at temperatures in the range of 0.32–0.77 of the melting temperature. Electron transparent samples were prepared by back etching and were examined in a transmission electron microscope. The details of the grain size measurements from the transmission electron micrographs as well as other experimental details can be found in Ref. [2].

Acknowledgements

R.B. and A.V. acknowledge support from the DFG under Grant No. Vo899/7. K.E. acknowledges support from the NSF under Grant No. DMR-0906676. We acknowledge computing resources at the JSC provided under grant HDR06. Part of the work has been done while A.V. was the guest of HIM at Universität Bonn and K.B., K.E. and A.V. were guests of IPAM at UCLA.

Appendix A. Supplementary material

Supplementary data associated with this article can be found, in the online version, at http://dx.doi.org/10.1016/j.actamat.2013.11.034.

References

[1] Herzer G. Modern soft magnets: amorphous and nanocrystalline materials. Acta Mater 2013;61:718.
[2] Barmak K, Eggeling E, Kinderlehrer D, Sharp R, Ta'asan S, Rollett A, et al. Grain growth and the puzzle of its stagnation in thin films: the curious tale of a tail and an ear. Prog Mater Sci 2013;58:987.
[3] Elsey M, Esedoglu S, Smereka P. Large-scale simulation of normal grain growth via diffusion-generated motion. Proc Roy Soc A 2011;467:381.
[4] Mullins W. Two-dimensional motion of idealized grain boundaries. J Appl Phys 1956;27:900.

[5] Herring C. Surface tension as a motivation for sintering. In: Kingston W, editor. The physics of powder metallurgy; 1951. p. 143.
[6] Winning M, Gottstein G, Shvindlerman L. Stress induced grain boundary motion. Acta Mater 2001;49:211.
[7] Holm E, Foiles S. How grain growth stops: a mechanism for grain-growth stagnation in pure materials. Science 2010;328:1138.
[8] Srinivasan S, Cahn J, Jonsson H, Kalonji G. Excess energy of grain-boundary trijunctions: an atomistic simulation study. Acta Mater 1999;47:2821.
[9] Upmanyu M, Srolovitz D, Shvindlerman L, Gottstein G. Molecular dynamics simulation of triple junction migration. Acta Mater 2002;50:1405.
[10] Cahn J, Taylor J. A unified approach to motion of grain boundaries, relative tangential translation along grain boundaries and grain rotation. Acta Mater 2004;52:4887.
[11] Shan Z, Stach E, Wiezorek J, Knapp J, Follstaadt D, Mao S. Grain boundary-mediated plasticity in nanocrystaline nickel. Science 2004;305:654.
[12] Upmanyu M, Srolovitz D, Lobkovsky A, Warren J, Carter W. Simultaneous grain boundary migration and grain rotation. Acta Mater 2006;54:1707.
[13] Trautt Z, Mishin Y. Grain boundary migration and grain rotation studied by molecular dynamics. Acta Mater 2012;60:2407.
[14] Mishin Y, Asta M, Li J. Atomistic modeling of interfaces and their impact on microstructure and properties. Acta Mater 2010;58:1117.
[15] Elder K, Katakowski M, Haataja M, Grant M. Modeling elasticity in crystal growth. Phys Rev Lett 2002;88:245701.
[16] Jaatinen A, Achim C, Elder K, Ala-Nissila T. Thermodynamics of bcc metals in phase-field-crystal models. Phys Rev E 2009;80:031602.
[17] Wu K-A, Voorhees P. Phase field crystal simulations of nanocrystalline grain growth in two dimensions. Acta Mater 2012;60:407.
[18] Boyer D, Vinals J. Weakly nonlinear theory of grain boundary motion in patterns with crystalline symmetry. Phys Rev Lett 2002;89:055501.
[19] Ohnogi H, Shiwa Y. Effect of noise on ordering of hexagonal grains in a phase-field-crystal model. Phys Rev E 2011;84:051603.
[20] Adland A, Xu Y, Karma A. Unified theoretical framework for polycrystalline pattern evolution. Phys Rev Lett 2013;110:265504.
[21] Bjerre M, Tarp J, Angheluta L, Mathiesen J. Rotation induced grain growth and stagnation in phase-field crystal models. Phys Rev E 2013;88:020401.
[22] Elder K, Provatas N, Berry J, Stefanovic P, Grant M. Phase-field crystal modeling and classical density functional theory of freezing. Phys Rev E 2007;75:064107.
[23] Wu K-A, Karma A. Phase-field crystal modeling of equilibrium bcc-liquid interfaces. Phys Rev B 2007;76:184107.
[24] van Teeffelen S, Backofen R, Voigt A, Loewen H. Derivation of the phase-field-crystal model for colloidal solidification. Phys Rev E 2009;79:051404.
[25] Ristau R, Barmak K, Coffey K, Howard J. Grain growth in ultra-thin films of CoPt and FePt. J Mater Res 1999;14:3263.
[26] Barmak K, Kim J, Kim C, Archibald W, Rohrer G, Rollett A, et al. Grain boundary energy and grain growth in Al films: comparison of experiments and simulations. Scripta Mater 2006;54:1059.
[27] Elsay M, Wirth B. An efficient simple scheme for phase field crystal simulation. ESAIM: Math Mod Numer Anal 2013;47:1413.
[28] Steinhardt P, Nelson D, Ronchetti M. Bond-orientational order in liquids and glasses. Phys Rev B 1983;28:784.